Published in "Superconductor Science and Technology 26(9): 095008, 2013"
which should be cited to refer to this work.

Effect of graphene oxide doping on superconducting properties of bulk MgB_2

Sudesh[1], N Kumar[2], S Das[3], C Bernhard[3] and G D Varma[1,2]

[1] Department of Physics, Indian Institute of Technology Roorkee, Roorkee-247667, India
[2] Centre of Nanotechnology, Indian Institute of Technology Roorkee, Roorkee-247667, India
[3] Department of Physics and Fribourg Centre for Nanomaterials-FriMat, University of Fribourg, Chemin du Musee 3, CH-1700 Fribourg, Switzerland

E-mail: gdvarfph@iitr.ernet.in

Abstract

In the present paper we report the effect of graphene oxide (GO) doping on the structural and superconducting properties of MgB_2. Bulk polycrystalline samples have been synthesized via a solid state reaction route with compositions $MgB_2 + x$ wt% of GO ($x = 0$, 1, 2, 3, 5, 7 and 10) by sintering at ~850 °C in a reducing atmosphere of Ar/H_2 (9:1). The x-ray diffraction results confirm the formation of the MgB_2 phase in all samples, together with traces of a MgO impurity phase. The XRD data results also show substitution of carbon for boron, but in the present case the actual amount of carbon substituting for boron is very small as compared to other carbon sources. A substantial improvement in the critical current density, $J_c(H)$, has been observed in the entire magnetic field range (0–8 T) for samples $x = 1$, 2 and 3 as compared to the undoped sample. In addition to $J_c(H)$, marginal improvements in the upper critical field (H_{c2}) and the irreversibility field (H_{irr}) have been observed for the doped samples $x = 1$, 2 and 3 with respect to pristine MgB_2. Furthermore, a curious result of the present investigation is that there is no change in the superconducting transition temperature (T_c) up to a doping level of 10 wt%. The possible mechanisms of flux pinning and correlations between the observed superconducting properties and structural characteristics of the samples have been described and discussed in this paper.

1. Introduction

Since the discovery of superconductivity at 39 K (T_c) in MgB_2 [1], much effort has been made to improve its superconducting properties. In addition to high T_c, large values of in-field critical current density ($J_c(H)$), upper critical magnetic field (H_{c2}) and irreversibility field (H_{irr}) are required for applications of superconducting material in high-field magnets. Unlike cuprate high-temperature superconductors, the absence of weak links [2, 3] at grain boundaries in MgB_2 makes it a potential candidate for technological applications. Very high critical current density, J_c values, ranging from 10^5 to 10^6 A cm^{-2}, in MgB_2 have been reported by several groups [4–8]. However, it has been found that J_c drops rapidly with increasing magnetic field due to poor flux pinning. Efforts are being made to improve all these properties by tuning the impurity scattering and introducing pinning centers into the samples by chemical doping. Most of the earlier element substitution studies were aimed at increasing T_c and thus were limited to low doping levels [9]. It has been suggested that a slight reduction in T_c corresponding to high levels of impurity phases is due to the fact that the inter-band scattering, which is responsible for T_c suppression by nonmagnetic impurities, is weak in the MgB_2 superconductor [10]. Therefore, chemical doping with nonmagnetic materials appears to be the most suitable approach to improve the superconducting properties of MgB_2 for practical applications. Carbon doping in MgB_2 using pure carbon as well as several carbon containing compounds, e.g. carbohydrates [11–13], B_4C [14], carbon-nanotubes [15], SiC [16] has been reported to be effective in improving superconducting properties such as H_{irr}, H_{c2} and J_c under

high magnetic fields. In addition to carbon, doping of rare earth oxides [17, 18], co-doping of rare earth and carbon [13] and magnetic nanoparticles [19] have also been found to be effective in improving the superconducting properties of MgB_2. In the case of carbon doping it has been found that carbon substituted at boron sites increases intra-band impurity scattering, leading to an enhancement in H_{c2} and a decrease in T_c. In addition to this, carbon doping also introduces defects in the sample, which act as pinning centers, leading to improvements in $J_c(H)$ and H_{irr} [20]. Recently, the effect of graphene doping on the superconducting properties of MgB_2 has been investigated [21–23]. A significant improvement in $J_c(H)$ has been found in graphene-doped MgB_2 without much reduction in T_c, in contrast to other carbon sources where 5–8 K reduction in T_c is observed. For example De Silva *et al* have shown an approximately 43-fold improvement in J_c at 5 K and 8 T field in 1% graphene-doped MgB_2 as compared to undoped MgB_2 [22]. Xu *et al* have reported an improvement in $J_c(H)$ by a factor of 30 at 5 K and 10 T field in 3.7 at.% doped MgB_2 with respect to undoped MgB_2 [23]. Thus, these recent reports show that graphene doping in MgB_2 provides efficient flux pinning, leading to improvements in J_c, and suggest a further detailed investigation on graphene-doped MgB_2 using a wider range of compositions of graphene would help to understand the pinning mechanism and effects of doping on superconducting properties such as T_c, H_{c2} and H_{irr}.

In light of this, in the present study we have synthesized graphene oxide (GO) doped MgB_2 with a wide wt% range of GO (0, 1, 2, 3, 5, 7 and 10 wt%) to study the effect of GO doping on the structural and superconducting properties of MgB_2. The main idea behind using GO as dopant in place of rGO is to avoid the additional process of reduction of GO into reduced graphene oxide (rGO). All samples have been sintered at 850 °C for 3 h in a reducing atmosphere of Ar/H_2 (9:1) with the aim to reduce the doped GO into rGO in the samples. We have found little change in the lattice parameters and almost no change in critical temperature T_c even up to 10 wt% doping. However, we have observed a substantial improvement in the critical current density over the entire range of magnetic fields (0–8 T) at 5 and 20 K for 1, 2 and 3 wt% GO-doped MgB_2 as compared to pristine MgB_2. Furthermore, we have observed a marginal improvement in H_{c2} and H_{irr} in the doped samples as compared to pristine samples. The possible mechanisms of flux pinning and correlations between the observed superconducting properties and structural characteristics of the samples are described and discussed in this paper.

2. Experimental details

Graphene oxide used in the present study for doping into the MgB_2 material was prepared using the method developed by Marcano *et al* [24]. Bulk polycrystalline samples of GO-doped MgB_2 were synthesized via a solid state reaction route with addition of the required amounts of GO in Mg and B. Appropriate amounts of Mg (Sigma Aldrich, 99.9% pure, grain size ~100 μm) and B (Sigma Aldrich, amorphous, 99%, grain size of submicron) to form MgB_2 were mixed with x wt% ($x = 0$, 1, 2, 3, 5, 7 and 10) of GO in an agate mortar. The mixture was thoroughly ground and the resulting powder was pressed to form rectangular pellets of dimension $7 \times 4 \times 1.5$ mm^3. The pellets were sintered at 850 °C in an Ar/H_2 (9:1) atmosphere for 3 h, followed by cooling down to room temperature by switching off the furnace. The phase identification of the samples was carried out using x-ray diffractometry with Cu Kα radiation. The microstructure of the samples was studied using a field emission scanning electron microscope (FESEM) and the elemental composition of the samples was checked using energy dispersive x-ray analysis (EDX). The quality of GO used for doping was checked by means of FTIR measurements. The resistivity measurement in different magnetic fields (0–8 T) was carried out using a physical properties measurement system (PPMS) (Quantum Design-6000) at the University of Fribourg. The irreversibility fields (H_{irr}) and upper critical field ($H_{c2}(T)$) were deduced using the criteria 10% and 90% of normal state resistivity for different applied fields, respectively. The DC magnetic measurements were carried out using a superconducting quantum interference device (SQUID) magnetometer (Quantum Design).

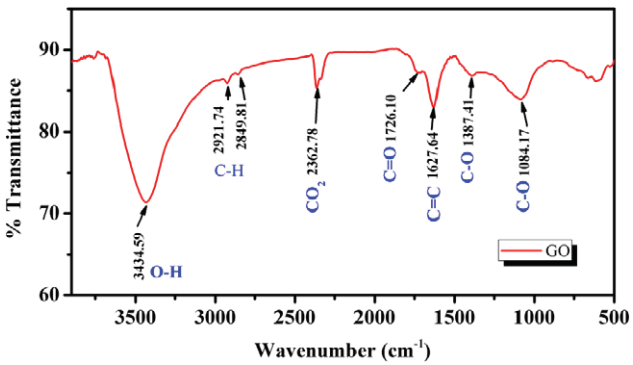

Figure 1. FTIR spectrum of graphene oxide prepared following the method developed by Marcano *et al* .

3. Results and discussion

Figure 1 shows the FTIR spectrum of graphene oxide prepared using the method developed by Marcano *et al* [24].

The FTIR spectrum of the GO sample accorded well with the previous works [25, 26]. Various oxygen configurations in the structure include the vibration modes of epoxide (C–O–C) (1230–1320 cm^{-1}), sp^2-hybrided C=C (1500–1600 cm^{-1}, in-plane vibrations), carboxyl (COOH) (1650–1750 cm^{-1} including C–OH vibrations at 3530 and 1080 cm^{-1}), ketonic species (C=O) (1600–1650 cm^{-1}, 1750–1850 cm^{-1}) and hydroxyl (namely phenol, C–OH) (3050–3800 cm^{-1} and 1070 cm^{-1}) with all C–OH vibrations from COOH and H_2O.

Figure 2 shows the x-ray diffraction patterns of $MgB_2 + x$ wt% GO samples with $x = 0$, 1, 2, 3, 5, 7 and 10. Except for a peak marked by * at $2\theta = 62.35°$ due to MgO, all peaks are well matched by the MgB_2 compound with space group *P6/mmm*. The volume percentage of the MgO phase formed in the samples is assessed from the sum of the relative x-ray

Table 1. Lattice parameters, estimated carbon content y, grain size, FWHM, strain, MgO content, T_c and $H_{c2}(0)$ of undoped and GO-doped samples.

x	a (Å)	c (Å)	y (%)	Grain size (μm)	FWHM (110)	Strain (%)	MgO (%)	T_c (K)	A_f	RRR	P (%)	$H_{c2}(0)$
0	3.0842	3.5257	0	0.330	0.1495	0.036	3.24	38.76	0.182	3.0993	43.6	16.95
1	3.0842	3.5252	0	0.293	0.1495	0.110	3.30	38.85	0.189	2.7380	43.4	17.31
2	3.0841	3.5253	0.09	0.282	0.1596	0.114	4.18	38.80	0.213	2.7434	47.6	18.05
3	3.0840	3.5254	0.12	0.279	0.1683	0.123	3.33	38.80	0.215	2.7418	51.3	17.45
5	3.0833	3.5244	0.35	0.241	0.1869	0.176	4.81	38.74	0.194	2.4051	48.7	16.78
7	3.0820	3.5244	0.76	0.243	0.1869	0.165	4.47	38.63	0.170	2.4275	44.6	16.12
10	3.0818	3.5225	0.82	0.242	0.1869	0.193	5.21	38.35	0.190	2.3522	47.2	15.15

peak intensities and tabulated in table 1. It has been found that the quantity of MgO present in the samples increases with increasing doping levels of GO. This is because of the increased amount of oxygen contained in the reaction mixture for higher GO content. Rietveld refinement was done using FullProf to determine the lattice parameters of the MgB_2 phase. The lattice parameters a and c of all samples are given in table 1. The lattice parameters observed for pure MgB_2 are $a = 3.0842$ Å and $c = 3.5259$ Å. We have seen a slight shift in the diffraction peaks towards higher angles (see inset of figure 2) with increasing GO concentration in the sample. This suggests a slight decrease in the lattice parameters of the doped samples as compared to the undoped samples (see table 1). The actual amount of carbon atoms (y) replacing the boron atoms in the MgB_2 system was calculated using the relation $a = 3.084\,39–0.3153y$ [27], where y is the carbon content given by $Mg(B_{1-y}C_y)_2$ and the results are given in table 1. Our result shows that in the case of GO-doped samples the amount of carbon doping is very small compared to that resulting from other carbon sources [11–16]. From the XRD patterns we have found a systematic increase in the full width at half maximum (FWHM) with increasing doping concentration of GO in the samples (see table 1), suggesting a decrease in the crystallite size and crystallinity of the samples due to doping of GO.

We have also calculated the strain in the samples from the Williamson–Hall plot [28] and the values are shown in table 1. We see that the strain increases with GO doping. This may be due to the different thermal expansion coefficient of MgB_2 and GO and also to the substitution of C for B. The microstructural characteristics of the samples have been studied by FESEM. The FESEM micrographs of samples $x = 0, 3, 7$ and 10 are shown in figures 3(a)–(d). From the micrographs it is clear that the doped samples are denser than the undoped one. Furthermore, in the doped samples the grains are well connected, and in some regions of the micrographs of the doped samples a film-like structure (shown by an arrow) of a few micron size is observed. The EDX data taken from this region shows a relatively higher carbon content as compared to other regions. For example, EDX data taken from the regions of box 1 and box 2 (film-like region) of figure 3(b) show ∼20% and ∼56% carbon, respectively. Although EDX does not give a correct analysis for light elements such as C, this analysis confirms that the film-like regions contain a higher carbon content as compared to other areas. This suggests that the film-like morphology may be due

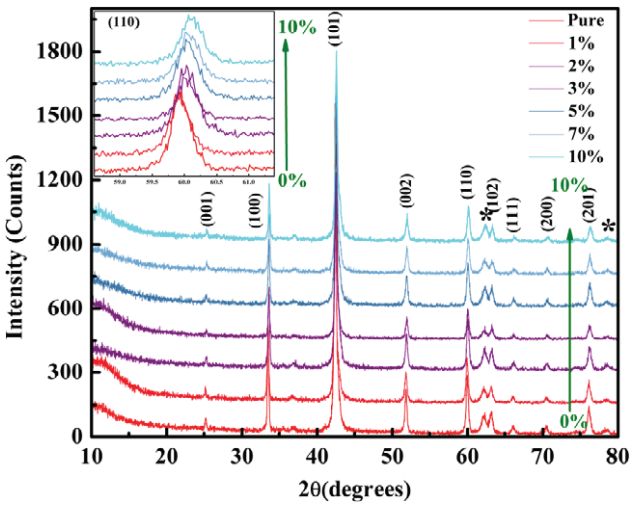

Figure 2. X-ray diffraction patterns of GO-doped MgB_2 samples, '*' shows the impurity peak of MgO. Inset shows shifting of the (110) peak with increasing doping level (x wt%) of GO.

to the presence of rGO in the samples. The average grain sizes of all samples obtained from the FESEM images are given in table 1. We see that grain size decreases with increasing doping level. This result is in accordance with the XRD result described above.

Figure 4 shows the normalized resistivity ($\rho(T)/\rho(300\ \text{K})$) versus temperature ($T$) plots in the temperature range 4–300 K for all $MgB_2 + x$ wt% GO samples with $x = 0, 1, 2, 3, 5, 7$ and 10 at zero applied field. The inset in this figure shows the normalized resistivity versus temperature plots of all samples at zero applied field in the vicinity of T_c.

The T_c values and residual resistivity ratio, $\rho(300\ \text{K})/\rho(40\ \text{K})$, (RRR), for these samples are shown in table 1. We notice that the resistivity of the samples increases with increased addition of GO into the system. This can be associated with the enhancement of electron scattering, consistent with the decrease of the RRR. According to Rowell, $\Delta\rho$ rather than RRR should be used to judge the intergrain connectivity in the samples [29]. Another important parameter is the effective superconducting cross-sectional area, A_f, which is used to estimate the connectivity of grains in the sample. The values of A_f for all samples have been calculated using the equation $A_f = \Delta\rho_{ideal}/(\rho(300\ \text{K}) - \rho(40\ \text{K}))$, proposed by Rowell [29]. Here, $\Delta\rho_{ideal}$ is the ideal relative

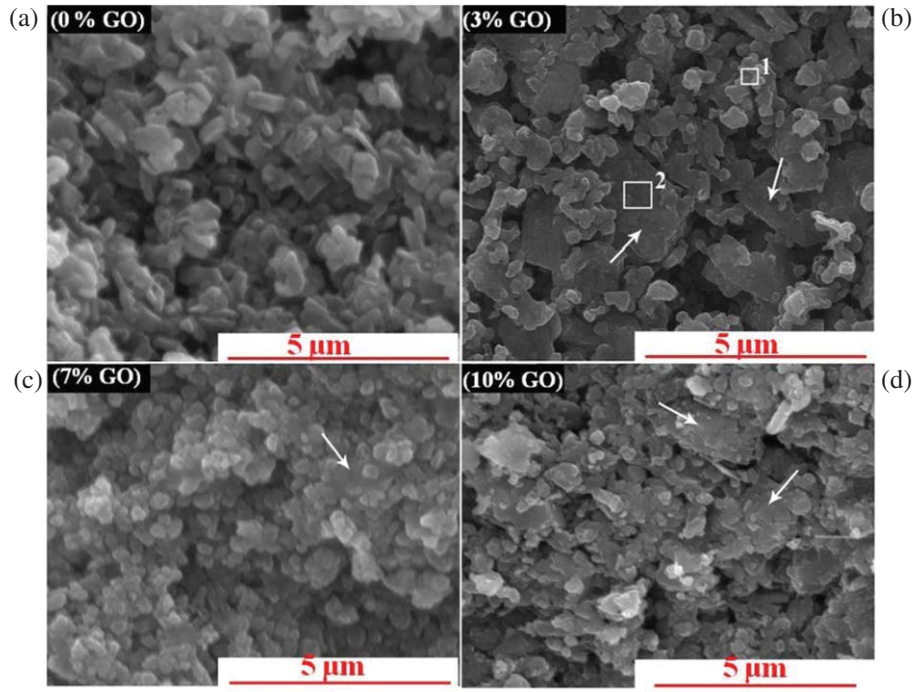

Figure 3. FESEM micrographs of GO-doped MgB_2 samples. (a) Pure, (b) 3 wt%, (c) 7 wt% and (d) 10 wt%. The boxes 1 and 2 in (b) show the regions from where EDX data have been taken.

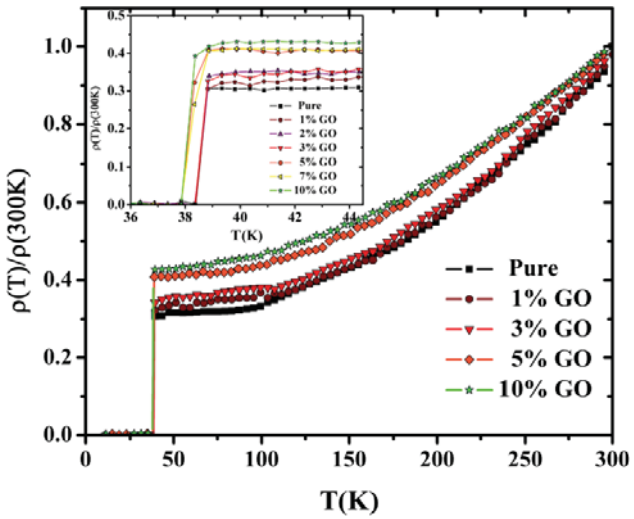

Figure 4. Normalized resistivity ($\rho(T)/\rho(300\ \mathrm{K})$) versus temperature ($T$) plots of $MgB_2 + x$ wt% GO samples with $x = 0$, 1, 3, 5 and 10 at zero applied field. Inset shows the superconducting transition in the temperature range 4–50 K for all the GO-doped and pure MgB_2 samples.

change in resistivity from 300 to 40 K for a fully connected sample and its value is taken as 7.3 $\mu\Omega$ cm [30]. The calculated values of A_f are shown in table 1. From the table we see that, apart from $x = 7$ wt%, the values of A_f for doped samples are higher as compared to that of undoped sample. This shows the better connectivity of the grains in the GO-doped samples. Furthermore, from the table we see that T_c is almost invariant with the doping level of GO. This result is similar to those reported on graphene-doped MgB_2 [22]. As reported, this may be due to a small substitution of carbon for boron (see table 1).

The resistivity versus temperature measurements for pure and GO-doped samples at different applied magnetic fields up to 8 T are shown in figure 5. The values of H_{c2} and H_{irr} were obtained from the resistivity transition of the samples using the criteria of 90% and 10% of normal state resistivity, respectively [31]. The upper critical field (H_{c2}) and irreversibility field (H_{irr}) values versus reduced temperature (T/T_c) for all the samples are shown in figures 6(a) and (b), respectively.

The H_{c2} curves show a positive curvature near T_c, which is in accordance with the two-band superconductivity in this system, as has been reported earlier [32]. The values of $H_{c2}(0)$ for the doped and undoped samples have been obtained by fitting the $H_{c2}(T)$ curves with Ginzburg–Landau theory [33]: $H_{c2}(T) = H_{c2}(0)[(1 - t^2)/(1 + t^2)]$, where $t = T/T_c$. Both H_{c2} and H_{irr} have shown an improvement with GO doping into the samples, with a maximum for 3 wt% GO doping into the MgB_2 sample. The $H_{c2}(0)$ value for the pure sample is found to be 16.95 T, increasing to 18.05 T with 3 wt% GO doping and then decreasing again to 15.15 T with 10 wt% GO doping. It has been reported that the enhancement in the upper critical field results from the reduction of the mean-free path of the charge carriers and the corresponding reduction of the coherence length [34]. The enhancement in H_{c2} observed in the present case is possibly due to lattice distortion created through GO doping that can lead to an enhanced impurity scattering. Such a distortion is evident from the increased FWHM. Furthermore, the carbon doping into the MgB_2 samples introduces electron scattering centers other than affecting the grain connectivity, thus increasing

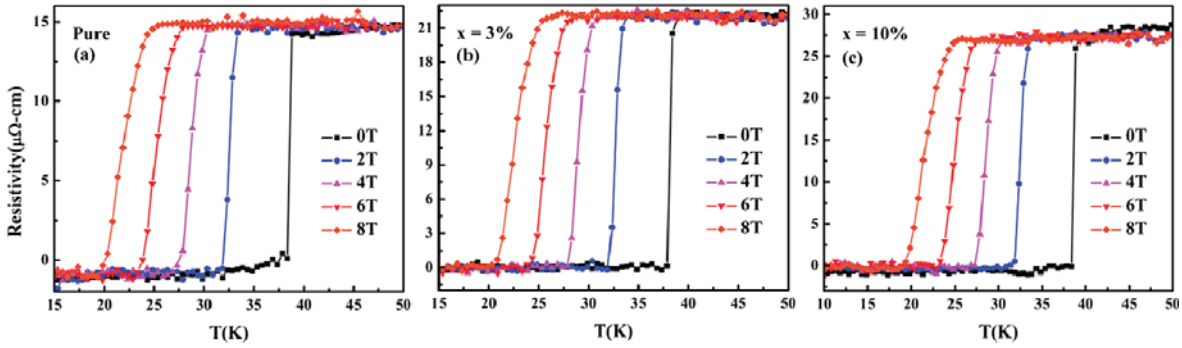

Figure 5. Superconducting transition zones of resistance versus temperature plots, at different applied fields (H) for (a) $x = 0$ wt%, (b) $x = 3$ wt% and (c) $x = 10$ wt% GO-doped MgB_2 samples.

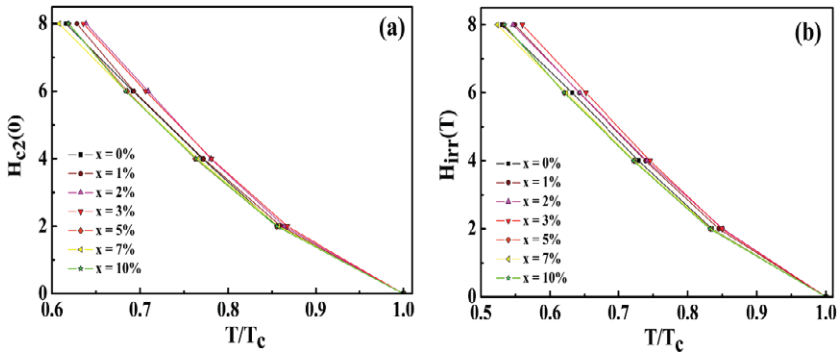

Figure 6. (a) $H_{c2}(T)$ versus reduced temperature (T/T_c) plots and (b) $H_{irr}(T)$ versus reduced temperature (T/T_c) plots for GO-doped and undoped MgB_2 samples.

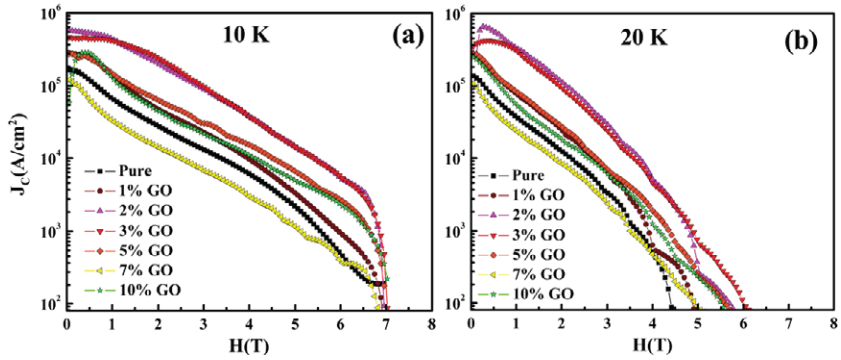

Figure 7. Field dependence of $J_c(H)$ of the GO-doped and undoped MgB_2 samples at (a) 10 K and (b) 20 K.

the resistivity and improving the upper critical field, H_{c2}. Figure 6(b) shows the H_{irr}–T plots for all the GO-doped samples. It is quite clear that the irreversibility in the samples has improved and reaches a value of 6 T at 24.7 K for the 3 wt% GO-doped sample before it decreases at higher doping. It may be due to increased flux pinning due to the presence of impurity phases rGO and MgO present at the grain boundaries. Thus, we see that the superconducting properties of MgB_2 improve due to doping of GO up to a doping level 3 wt%, and beyond this the properties start deteriorating. This may be due to increased disorder in the samples having higher GO contents.

The field-dependent magnetization ($M(H)$) of all samples has been measured at 10 and 20 K. Figures 7(a) and (b) show the $J_c(H)$ curves at 10 K and 20 K, respectively, for all the GO-doped samples obtained from the $M(H)$ curves using Bean's critical state model [35]: $J_c = 20\Delta M/[Va(1 - a/3b)]$, where ΔM is the width of the magnetic hysteresis loop and V, a and b are the volume, width and length of the sample, respectively. The J_c shows an exponential decrease with increasing magnetic field in low as well as in high magnetic fields. It is clear from the figure that the J_c value for $x = 3$ wt% attains the highest value among the samples for temperatures of both 10 and 20 K in the entire applied field range. The values of J_c for self-field and at 5 T (10 K) and 4 T (20 K) are shown in table 2. The J_c values obtained in the present case are comparable to the results of recent reports on graphene-doped MgB_2 superconductor [22]. However, the values of J_c are

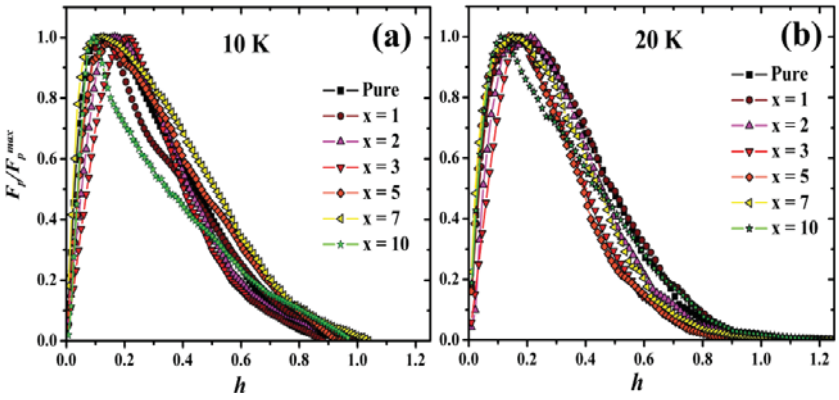

Figure 8. F_p/F_p^{max} versus h plots of GO-doped and undoped MgB_2 samples at (a) 10 K and (b) 20 K.

Table 2. Fitting parameters obtained by fitting the pinning force density versus reduced field plots.

	$f_p^{mod} = \alpha H \exp(-(H/H1)^{n1}) + \beta H(-(H/H2)^{n2})$								J_c (A cm^{-2})			
	10 K				20 K				10 K		20 K	
x (%)	$H1$	$n1$	$H2$	$n2$	$H1$	$n1$	$H2$	$n2$	0 T ($\times 10^5$)	5 T ($\times 10^3$)	0 T ($\times 10^5$)	4 T ($\times 10^3$)
0	0.77	1.04	3.72	2.66	0.43	0.97	2.04	2.09	1.65	2.01	1.39	0.51
1	1.01	2.02	2.70	1.86	0.44	1.21	1.66	1.71	2.79	3.08	2.68	0.64
2	1.41	2.88	2.14	1.47	0.77	3.63	1.48	1.55	5.75	13.62	2.83	5.08
3	2.06	2.58	3.02	1.92	1.19	3.00	1.84	1.86	4.57	13.50	3.56	4.56
5	1.04	1.33	3.68	2.34	0.40	2.14	1.17	1.25	2.71	6.24	2.74	1.89
7	0.45	1.00	2.76	1.84	0.30	0.72	2.22	2.38	1.21	1.09	1.09	0.48
10	0.95	2.82	1.72	1.16	0.53	1.41	1.20	1.80	0.58	4.67	2.46	1.26

lower than SiC-doped MgB_2 [36]. For example, for 10% SiC-doped sample, the value of J_c is 3.6×10^4 A cm^{-2} at 4 T (20 K), whereas in the present case for 3% GO-doped samples, J_c is $\sim 0.5 \times 10^4$ A cm^{-2} at 4 T (20 K).

In previous studies, it has been reported that the critical current density in MgB_2 superconductors is considerably influenced by the porous microstructure of these materials [37] and it has been deduced that J_c can be effectively improved by reducing the porosity in the samples, thus improving its packing factor and connectivity. In the present case, we have calculated the packing factor, P, for all the samples, following the method given by Yamamoto *et al* [37]. The values of P are listed in table 1. We observe a significant improvement in the packing factor of doped samples as compared to the undoped sample. Thus effect of doping on P is similar to that on J_c, which indicates a direct correlation between J_c and P. This is consistent with the results reported by Yamamoto *et al*.

In order to study the behavior of flux pinning in the samples, we have plotted the reduced flux pinning force density ($f_p = F_p/F_p^{max}$, where $\vec{F}_p = \vec{J}_c \times \vec{H}$) as a function of the magnetic field for all samples at 10 K and 20 K, as shown in figures 8(a) and (b), respectively. Here, F_p and F_p^{max} are, respectively, the global flux pinning force density and its maximum value. Much research work has been done to study the mechanism of flux pinning in superconducting MgB_2 samples. The model developed by Fitz and Webb [38] for the flux pinning force density, f_p, is mostly employed to deduce the pinning mechanism in polycrystalline MgB_2 samples. In this model, f_p is given by $f_p = h^p(1-h)^q$, where p and q are shape parameters depending on the nature of defects present in the material which give rise to pinning behavior in the samples, and h is the reduced field, $h = H/H_{irr}$. In the present case, the H_{irr} values have been obtained by a linear extrapolation to zero of the low-J_c segment of the Kramer plot [39], i.e. $F_k = J_c^{1/2}H^{1/4}(H)$ versus reduced field (h) plot, which is considered to be the most convincing method to estimate the value of H_{irr}. To observe the type of pinning present in the samples, we have tried to fit the $f_p(h)$ curves with scaling laws. The attempts to fit the $f_p(h)$ curves with the general scaling model $f_p(h) = h^p(1-h)^q$ fail to describe correctly both the peak and high-field region. This is mainly because this model works for the isotropic case and does not take into account the anisotropy, the defects present in polycrystalline samples and their porous microstructure [37].

Horvat *et al* [40, 41] have reported that the value of J_c calculated from magnetic measurements carries with it the effect of the porous nature of MgB_2 samples. It has been reported that the presence of voids leads to superconducting screening at two different length scales [40]. Both these screening currents have a different magnetic field dependence, so they are considered to have different contributions to the magnetic moment and thus to the magnetic critical current density. Therefore, the critical current density can be expressed as a stretched exponential function given by [42]:

$$J_c = \alpha \exp\left(-\left(\frac{H}{H1}\right)^{n1}\right) + \beta \exp\left(-\left(\frac{H}{H2}\right)^{n2}\right) \quad (1)$$

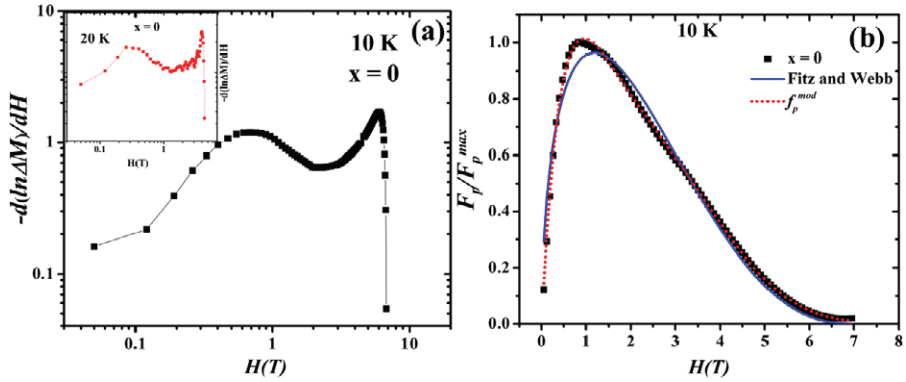

Figure 9. (a) Variation of $-\mathrm{d}(\ln(\Delta M))/\mathrm{d}H$ with applied magnetic field at 10 K for pure MgB_2. The inset of this figure shows the plot at 20 K for the same sample. (b) Fitting of pinning force density, f_p, with Fitz and Webb's model (solid line) and f_p^{mod} (dotted line) at 10 K for the pure MgB_2 sample.

where $\alpha, \beta, H1, H2$ and $n1, n2$ are fitting parameters. The parameters α and β contain the contributions of the two screening currents in the samples. Here the stretched exponential function was chosen because the experimental points fall on a straight line when plotted in a $-\mathrm{d}(\ln(\Delta M))/\mathrm{d}H$ versus H plot with log–log scales [40], where ΔM is the width of the $M(H)$ loop. Similar behavior is observed in the present case, as shown in figure 9(a). In the present case we have used the following modified form of f_p^{mod} to fit the reduced pinning force density versus H plots on the basis of the above form of J_c as $F_p = JH$.

$$f_p^{mod} = \alpha H \exp\left(-\left(\frac{H}{H1}\right)^{n1}\right) + \beta H \exp\left(-\left(\frac{H}{H2}\right)^{n2}\right). \quad (2)$$

We show in figure 9(b) the fitting of experimental data using the above form of f_p^{mod} (equation (2)) for the sample $x = 0$. The fitting parameters are shown in table 2. The comparison of fittings by the form of f_p given by Fitz and Webb and by stretched exponential form is shown in figure 9(b). From figure 9(b), we find excellent fitting with f_p^{mod}. This result suggests that different superconducting screenings due to irregularities in the present samples are more likely the reason for better fitting success with double-exponential function.

4. Conclusion

In the present work, we have studied the effect of GO doping on the superconducting properties of the MgB_2 compound. The superconducting critical current density is significantly improved with GO doping into the sample over the entire magnetic field range (0–8 T) without affecting the transition temperature up to a doping level of 3 wt%. The upper critical field and irreversibility field are also improved. The maximum $H_{c2}(0)$ as calculated from Ginzburg–Landau fit is found to be 18.05 T for 3 wt% GO-doped MgB_2. Further, we have observed excellent fittings of the reduced pinning force density versus H plots by a stretched double-exponential function that takes into account the anisotropy and porous microstructure of the MgB_2 samples.

Acknowledgments

Two of the authors, Sudesh and N Kumar are grateful to the Ministry of Human Resources and Development (MHRD) and the Council of Scientific and Industrial Research (CSIR), India, respectively, for providing financial support. S Das and C Bernhard acknowledge funding by the Swiss National Science Foundation (SNF) Grant No. 200020-140225 and by Project No. 122935 of the Indo-Swiss Joint Research Program (ISJRP).

References

[1] Nagamatsu J, Nakagawa N, Muranaka T, Zenitani Y and Akimitsu J 2001 *Nature* **410** 63
[2] Larbalestier D C *et al* 2001 *Nature* **410** 186
[3] Bugoslavsky Y, Perkins G K, Qi X, Cohen L F and Caplin A D 2001 *Nature* **410** 563
[4] Grasso G, Malagoli A, Ferdeghini C, Roncallo S, Braccini V, Siri A S and Cimberle M R 2001 *Appl. Phys. Lett.* **79** 230
[5] Jin C Q, Li S C, Zhu J L, Li F Y, Liu Z X and Yu R C 2002 *J. Mater. Res.* **17** 525
[6] Goldacker W, Schlachter S I, Zimmer S and Reiner H 2001 *Supercond. Sci. Technol.* **14** 787
[7] Glowacki B A, Majoros M, Vickers M, Evetts J E, Shi Y and McDougall I 2001 *Supercond. Sci. Technol.* **14** 193
[8] Moon S H, Yun J H, Lee H N, Kye J I, Kim H G, Chung W and Oh B 2001 *Appl. Phys. Lett.* **79** 2429
[9] Goto D, Machi T, Zhao Y, Koshizuka N, Murakami M and Arai S 2003 *Physica* C **392–396** 272
[10] Mazin I I, Andersen O K, Jepsen O, Dolgov O V, Kortus J, Golubov A A, Kuzmenko A B and van der Marel D 2002 *Phys. Rev. Lett.* **89** 107002
[11] Kim J H, Zhou S, Hossain M S A, Pan A V and Dou S X 2006 *Appl. Phys. Lett.* **89** 142505
[12] Ojha N, Malik V K, Singla R, Bernhard C and Varma G D 2009 *Supercond. Sci. Technol.* **22** 125014
[13] Ojha N, Malik V K, Singla R, Bernhard C and Varma G D 2010 *Supercond. Sci. Technol.* **23** 045005
[14] Yamamoto A, Shimoyama J, Ueda S, Iwayama I, Horii S and Kishio K 2005 *Supercond. Sci. Technol.* **18** 1323
[15] Yeoh W K, Horvat J, Kim J H, Xu X and Dou S X 2007 *IEEE Trans. Appl. Supercond.* **17** 2929
[16] Vajpayee A, Jha R, Srivastava A K, Kishan H, Tropeano M, Ferdeghini C and Awana V P S 2011 *Supercond. Sci. Technol.* **24** 045013

[17] Ojha N, Malik V K, Bernhard C and Varma G D 2009 *Physica* C **469** 846
[18] Gao Z, Wang D, Zhang X, Ma Y, Awaji S, Nishijima G, Watanabe K and Flukiger R 2010 *Supercond. Sci. Technol.* **23** 045024
[19] Qu B, Sun X D, Li J G, Xiu Z M, Liu S H and Xue C P 2009 *Supercond. Sci. Technol.* **22** 015027
[20] Dou S X, Pan A V, Zhou S, Ionescu M, Wang X L, Horvat J, Liu H K and Munroe P R 2003 *J. Appl. Phys.* **94** 1850
[21] De Silva K S B, Xu X, Li W X, Zhang Y, Rindfleisch M and Tomsic M 2011 *IEEE* **21** 2686
[22] De Silva K S B, Gambhir S, Wang X L, Xu X, Li W X, Officer D L, Wexler D, Wallace G G and Dou S X 2012 *J. Mater. Chem.* **22** 13941
[23] Xu X, Dou S X, Wang X L, Kim J H, Stride J A, Choucair M, Yeoh W K, Zheng R K and Ringer S P 2010 *Supercond. Sci. Technol.* **23** 085003
[24] Marcano D C, Kosynkin D V, Berlin J M, Sinitskii A, Sun Z, Slesarev A, Alemany L B, Lu W and Tour J M 2010 *ACS Nano* **4** 4806
[25] Pham V H, Cuong T V, Hur S H, Oh E, Kim E J, Shin E W and Chung J S 2011 *J. Mater. Chem.* **21** 3371
[26] Nethravathi C and Rajamathi M 2008 *Carbon* **46** 1994
[27] Senkowicz B J, Giencke J E, Patnaik S, Eom C B, Hellstrom E E and Larbalestier D C 2005 *Appl. Phys. Lett.* **86** 202502
[28] Williamson G K and Hall W H 1953 *Acta Metall.* **1** 22
[29] Rowell J M 2003 *Supercond. Sci. Technol.* **16** R17–27
[30] Canfield P C, Finnemore D K, Bud'ko S L, Ostenson J E, Lapertot G, Cunningham C E and Petrovic C 2001 *Phys. Rev. Lett.* **86** 2423
[31] Zhang X, Ma Y, Gao Z, Wang D, Yu Z and Wang L 2007 *Supercond. Sci. Technol.* **20** 1198
[32] Gurevich A 2003 *Phys. Rev.* B **67** 184515
[33] Wang X, Ghorbani S R, Peleckis G and Dou S X 2009 *Adv. Mater.* **21** 236
[34] Kaushik S D, Kumar R, Mishra P K, Giencke J E, Kim D M, Eom C B and Patnaik S 2006 *Physica* C **442** 73
[35] Bean C P 1964 *Rev. Mod. Phys.* **36** 31
[36] Dou S X, Soltanian S, Horvat J, Wang X L, Zhou S H, Ionescu M, Liu H K, Munroe P and Tomsic M 2002 *Appl. Phys. Lett.* **81** 3419
[37] Yamamoto A, Jun-ichi S, Kishio K and Matsushita T 2007 *Supercond. Sci. Technol.* **20** 658
[38] Fietz W A and Webb W W 1969 *Phys. Rev.* **178** 657
[39] Kramer E J 1973 *J. Appl. Phys.* **44** 1360
[40] Horvat J, Soltanian S, Wang X L and Dou S X 2004 *Appl. Phys. Lett.* **84** 3109
[41] Horvat J, Soltanian S, Pan A V and Wang X L 2004 *J. Appl. Phys.* **96** 4342
[42] Horvat J, Yeoh W K, Kim J H and Dou S X 2008 *Supercond. Sci. Technol.* **21** 065003